Mecánica Computacional Vol. XXI, pp. 652–669
S. R. Idelsohn, V. E. Sonzogni and A. Cardona (Eds.)
Santa Fe–Paraná, Argentina, October 2002

# NUMERICAL SIMULATION OF WAVES IN POROVISCOELASTIC ROCKS SATURATED BY IMMISCIBLE FLUIDS

**Juan E. Santos*, Patricia M. Gauzellino†, and Claudia L. Ravazzoli†**

*Facultad de Ciencias Astronómicas y Geofísicas,
Universidad Nacional de La Plata, CONICET
Paseo del Bosque s/n, 1900 - La Plata, Argentina
e-mail: santos@fcaglp.fcaglp.unlp.edu.ar
Also Department of Mathematics, Purdue University, W. Lafayette, IN, 47907, USA

†Facultad de Ciencias Astronómicas y Geofísicas,
Universidad Nacional de La Plata
Paseo del Bosque s/n, 1900 - La Plata, Argentina
Also Facultad de Ingeniería, UNLP
e-mail: gauze@fcaglp.fcaglp.unlp.edu.ar

†Facultad de Ciencias Astronómicas y Geofísicas,
Universidad Nacional de La Plata, CONICET
e-mail: claudia@fcaglp.fcaglp.unlp.edu.ar

**Key Words:** wave propagation, Biot's media, domain decomposition, finite elements

**Abstract.** *Using a generalization of Biot's theory, we represent wave propagation in a porous solid saturated by a two-phase fluid. This theory predicts the existence of one shear wave and three compressional waves (one fast wave and two slow waves). The model takes into account capillary forces and viscous and mass coupling interaction coefficients between the fluid phases under variable saturation and pore fluid pressure conditions. Dissipative effects and viscoelasticity are also included in the formulation. The numerical procedure is an iterative domain decomposition algorithm formulated in the space–frequency domain and is specifically designed for implementation in parallel architectures. We perform numerical experiments in a real sandstone saturated by two fluids (gas-water) and analyze the wave fields obtained at ultrasonic frequencies.*

## 1 INTRODUCTION

An important topic in exploration geophysics is seismic forward modeling, which involves an understanding of the seismic response of stratigraphic features in reservoirs and may provide useful information about rocks and saturant fluid properties.

Although several authors have studied wave propagation in porous rocks saturated by fluids,[1–7] those theories do not include variable pressure conditions nor capillary pressure effects. We present a model that is according to Biot's theory and takes into account capillary forces and viscous and mass coupling interaction coefficients between the fluid phases under variable saturation and pore fluid pressure conditions. Frequency dependent dissipative effects associated to viscous forces and viscoelasticity are also included in the formulation.

In a porous solid saturated by a single phase fluid, the classical theory of Biot predicts one shear wave and two compressional waves, Type I or "fast" and Type II or "slow".[1,2,8] The Type II Biot wave was observed by Plona[9] in the laboratory and in different numerical simulations.[10–13]

In a porous solid saturated by a two-phase fluid, a second slow compressional mode (Type III) can propagate. Various works[14–16] provide evidence that for the low frequency range, the two slow modes are diffuse waves due to viscous effects. While, under very high frequencies, such as those used in laboratory testing, these two modes clearly are propagating waves.

Naturally, the space–frequency domain is chosen to describe phenomena of dissipation and anelastic attenuation suffered by the different type of waves. Moreover, this domain allows to compute the solution at the current time without the knowledge of the time history of the system, that is, the solution is computed for each temporal frequency and a finite number of them are required to obtain the solution in the space–time domain via inverse Fourier transform.[17–19]

Here, the numerical procedure is an iterative nonoverlapping domain decomposition algorithm. As it is known, domain decomposition avoids the construction of a large linear system related to any global finite element technique and is suited to distribute data among the processors in a distributed memory computer. This implementation is related to numerous works on the subject.[20–25] We use the nonconforming rectangular finite element presented in[26] to approximate the solid displacement vector, and the vector part of the Raviart-Thomas-Nedelec mixed finite element space of order zero to approximate the displacement of the two fluid phases, which are conforming spaces, see.[27,28]

Finally, we applied our algorithm and performed numerical experiments in a real sandstone saturated by two fluids (gas–water). We analyzed snapshots and traces of the wave fields obtained in the different phases at ultrasonic frequencies. As the second slow wave has not been observed in the laboratory yet, then this modelling method can be useful for devising laboratory experiments appropriate to this purpose.

## 2 GOVERNING EQUATIONS

The governing equations for wave propagation in the space–frequency domain are the equations of motion given in[29]

$$\begin{aligned} -\omega^2 \left(\rho\, u^s + \rho_n\, \bar{S}_n u^n + \rho_w\, \bar{S}_w\, u^w\right) - \nabla \cdot \tau(u) &= f^s, \\ -\omega^2 \left(\rho_n\, \bar{S}_n\, u^s + g_n\, u^n + g_{nw}\, u^w\right) + i\omega\, d_n\, u^n - i\omega\, d_{nw}\, u^w + \nabla \mathcal{T}_n(u) &= f^n, \\ -\omega^2 \left(\rho_w\, \bar{S}_w\, u^s + g_{nw}\, u^n + g_w\, u^w\right) + i\omega\, d_w\, u^w - i\omega\, d_{nw}\, u^n + \nabla \mathcal{T}_w(u) &= f^w. \end{aligned} \tag{1}$$

In the porous solid saturated by two immiscible fluids, we consider a *wetting* phase and a *non-wetting* one, which will be indicated with the subscripts (or superscripts) "$w$" and "$n$", respectively. The Fourier transform of the averaged displacement vectors for the solid and the fluid phases at the angular frequency $\omega$ are $u^s$, $u^n$, and $u^w$. The coefficient $\rho$ is the density of the bulk material given by $\rho = (1-\phi)\rho_s + \phi\left(\bar{S}_n\rho_n + \bar{S}_w\rho_w\right)$, where $\phi$ is the matrix effective porosity, $\rho_s$ is the mass density of the solid grains, $\rho_n$, $\rho_w$ are the mass densities of the fluids, with $\bar{S}_n$ and $\bar{S}_w$ being the averaged fluid saturations. The two fluid phases completely saturate the porous part of the matrix and also both fluids are allowed to move inside the pore space.

The mass coupling coefficients $g_n$, $g_w$, $g_{nw}$ represent the inertial effects associated with dynamic interactions between the three different phases, while the coefficients $d_n$, $d_w$ and $d_{nw}$ include the viscous coupling effects between the solid and fluid phases.

The external source in the solid and fluid phases are represented by $f^s$, $f^n$ and $f^w$, respectively.

The constitutive equations are given by Santos & Ravazzoli[16]

$$\begin{aligned} \tau_{ij}(u) &= 2N\,\varepsilon_{ij} + \delta_{ij}(\lambda_c\, e_b - B_1\,\xi^n - B_2\,\xi^w), \\ \mathcal{T}_n(u) &= \left(\bar{S}_n + \beta + \zeta\right) P_n - (\beta+\zeta)\, P_w = -B_1\, e_b + M_1\,\xi^n + M_3\,\xi^w, \\ \mathcal{T}_w(u) &= \left(\bar{S}_w + \zeta\right) P_w - \zeta\, P_n = -B_2\, e_b + M_3\,\xi^n + M_2\,\xi^w, \end{aligned} \tag{2}$$

where $\tau$, $\mathcal{T}_n$ and $\mathcal{T}_w$ are the generalized stresses of the system. The coefficients $N, \lambda_c, B_1, B_2, M_1, M_2, M_3$ are the elastic moduli of the medium, depending on saturation, capillary pressure, wetting fluid pressure, porosity, the bulk and shear moduli of the frame and solid grains and the bulk moduli of both fluids. $\varepsilon_{ij}$ and $e_b = \varepsilon_{ii}$ are the Fourier transforms of the strain tensor of the solid and its linear invariant, respectively and $\xi^\theta = -\nabla \cdot u^\theta$, for $\theta = n, w$. $P_w$ and $P_n$ denote infinitesimal changes in the pressures of the wetting and non-wetting fluids, respectively, with respect to corresponding reference values $\bar{P}_n$, and $\bar{P}_w$ associated with the initial equilibrium state with corresponding nonwetting fluid saturation $\bar{S}_n$, where $P_n$ and $P_w$ are related through the capillary relation.[30–32] The values $\beta$ and $\zeta$ are related to the capillary pressure.[29]

We use the Correspondence Principle stated by M. Biot[3,8] to introduce viscoelasticity, i.e. replacing the real poroelastic coefficients in the constitutive relations by complex frequency dependent poroviscoelastic moduli satisfying the same relations as in the elastic case, with some necessary thermodynamic restrictions. Other mechanisms of wave

attenuation are associated to viscous drag between the fluid and the solid matrix which are also related to the relative permeability functions.[16,33] The viscodynamic correction factors for high frequencies are computed by generalizing the corresponding ones for the single–phase fluid case.

The whole set of complex poroviscoelastic moduli and coefficients are derived in.[29]

## 3 DOMAIN DECOMPOSITION METHOD

### 3.1 Multi-domain formulation

Domain decomposition method is based on partitions of the computational domain into subdomains without overlap. We assume that $\Omega$ in the $(x,z)$–plane is partitioned into subdomains $\Omega_j$ such that $\Omega = \cup_{j=1}^{J} \Omega_j$ and denote the boundaries by $\Gamma_j := \partial\Omega \cap \partial\Omega_j$ and $\Gamma_{jk} := \partial\Omega_j \cap \partial\Omega_k$ as the common interface between two adjoining subdomains $\Omega_j$ and $\Omega_k$.

We indicate by $u_j$ the restriction to $\Omega_j$ of the solution $u = (u^s, u^n, u^w)$ to (2.1), and by $\nu_{jk}$ the unit outer normal on $\Gamma_{jk}$ from $\Omega_j$ to $\Omega_k$ and by $\nu_j$ the unit outer normal to $\Gamma_j$. Also indicate $\xi_j$ and $\xi_{jk}$ the midpoints of $\Gamma_j$ and $\Gamma_{jk}$, respectively.

Now, we reformulate our problem in the equivalent multi-domain form: find $u_j(x,z,\omega)$, for $j = 1, \cdots, J$

$$\begin{aligned} -\omega^2 \left(\rho\, u_j^s + \rho_n\, \bar{S}_n u_j^n + \rho_w\, \bar{S}_w\, u_j^w\right) - \nabla\cdot\tau(u_j) &= f^s, \\ -\omega^2 \left(\rho_n\, \bar{S}_n\, u_j^s + g_n\, u_j^n + g_{nw}\, u_j^w\right) + i\omega\, d_n\, u_j^n - i\omega\, d_{nw}\, u_j^w + \nabla\mathcal{T}_n(u_j) &= f^n, \\ -\omega^2 \left(\rho_w\, \bar{S}_w\, u_j^s + g_{nw}\, u_j^n + g_w\, u_j^w\right) + i\omega\, d_w\, u_j^w - i\omega\, d_{nw}\, u_j^n + \nabla\mathcal{T}_w(u_j) &= f^w. \end{aligned} \tag{3}$$

This system requires consistency conditions that satisfy a suitable matching on $\Gamma_{jk}$,

$$\begin{aligned} u_j^s = u_k^s, \quad u_j^n\cdot\nu_{jk} = -u_k^n\cdot\nu_{kj}, \quad u_j^w\cdot\nu_{jk} = -u_k^w\cdot\nu_{kj}, \\ \tau(u_j)\nu_{jk} = -\tau(u_k)\nu_{kj}, \quad \mathcal{T}_n(u_j) = \mathcal{T}_n(u_k), \quad \mathcal{T}_w(u_j) = \mathcal{T}_w(u_k) \quad , (x,z)\in\Gamma_{jk}. \end{aligned} \tag{4}$$

Also, we impose the first-order absorbing boundary conditions based on the conservation of momentum

$$(-\tau(u_j)\nu_j\cdot\nu_j, \tau(u_j)\nu_j\cdot\chi_j, \mathcal{T}^n, \mathcal{T}^w) = i\omega\mathcal{B}\left(u_j^s\cdot\nu_j, u_j^s\cdot\chi_j, u_j^n\cdot\nu_j, u_j^w\cdot\nu_j\right),\ (x,z)\in\Gamma_j \tag{5}$$

where $\chi_j$ is a unit tangent on $\Gamma_j$ so that $\{\nu_j, \chi_j\}$ form an orthonormal system on $\Gamma_j$ and the symmetric positive definite matrix $\mathcal{B}$ is given by[34]

$$\mathcal{B} = \left[\left(\mathcal{A}^{-1}\mathcal{E}\right)^t\right]^{\frac{1}{2}} \mathcal{A} = \mathcal{A}^{\frac{1}{2}}\,\mathcal{D}^{\frac{1}{2}}\,\mathcal{A}^{\frac{1}{2}}, \quad \mathcal{D} = \mathcal{A}^{-\frac{1}{2}}\mathcal{E}\mathcal{A}^{-\frac{1}{2}},$$

where $\mathcal{A}$ and $\mathcal{E}$ are matrices whose entries depend on the physical properties of the medium, see.[29]

We will replace the expressions (3.2) by the equivalent Robin transmission boundary conditions

$$\begin{aligned}
&(\tau(u_j)\nu_{jk}\cdot\nu_{jk}, \tau(u_j)\nu_{jk}\cdot\chi_{jk}, -\mathcal{T}_n(u_j), -\mathcal{T}_w(u_j)) \\
&\qquad +i\omega\beta_{jk}\left(u_j^s\cdot\nu_{jk}, u_j^s\cdot\chi_{jk}, u_j^n\cdot\nu_{jk}, u_j^w\cdot\nu_{jk}\right) \\
&= (\tau(u_k)\nu_{kj}\cdot\nu_{kj}, \tau(u_k)\nu_{kj}\cdot\chi_{kj}, -\mathcal{T}_n(u_k), -\mathcal{T}_w(u_k)) \\
&\qquad -i\omega\beta_{jk}\left(u_k^s\cdot\nu_{kj}, u_k^s\cdot\chi_{kj}, u_k^n\cdot\nu_{kj}, u_k^w\cdot\nu_{kj}\right) \qquad (x,z)\in\Gamma_{jk}\subset\partial\Omega_j,
\end{aligned} \tag{6}$$

and

$$\begin{aligned}
&(\tau(u_k)\nu_{kj}\cdot\nu_{kj}, \tau(u_k)\nu_{kj}\cdot\chi_{kj}, -\mathcal{T}_n(u_k), -\mathcal{T}_w(u_k)) \\
&\qquad +i\omega\beta_{jk}\left(u_k^s\cdot\nu_{kj}, u_k^s\cdot\chi_{kj}, u_k^n\cdot\nu_{kj}, u_j^w\cdot\nu_{kj}\right) \\
&= (\tau(u_j)\nu_{jk}\cdot\nu_{jk}, \tau(u_j)\nu_{jk}\cdot\chi_{jk}, -\mathcal{T}_n(u_j), -\mathcal{T}_w(u_j)) \\
&\qquad -i\omega\beta_{jk}\left(u_j^s\cdot\nu_{jk}, u_j^s\cdot\chi_{jk}, u_j^n\cdot\nu_{jk}, u_j^w\cdot\nu_{jk}\right) \qquad (x,z)\in\Gamma_{jk}\subset\partial\Omega_k.
\end{aligned} \tag{7}$$

Here $\beta_{jk}$ is a positive definite matrix function defined on the interior boundaries $\Gamma_{jk}$ and $\chi_{jk}$ is a unit tangent on $\Gamma_{jk}$ so that $\{\nu_{jk}, \chi_{jk}\}$ form an orthonormal system on $\Gamma_{jk}$.

### 3.2 Variational formulation and iterations

In view of an iterative technique, we denote $u_j^t = (u_j^{s,t}, u_j^{n,t}, u_j^{w,t})$ as the solution of the problem at the $t$-iteration level, $t = 0, 1, 2, \cdots$, and assume that the variables $u_k$ in the Robin transmission condition are those corresponding to the previous iteration level $t-1$.

In order to formulate the problem in a variational way, we introduce Sobolev spaces. $H^1(\Omega_j)$ denotes the usual Sobolev space of functions in $L^2(\Omega_j)$ with first derivatives in $L^2(\Omega_j)$ and also $H(div, \Omega_j) = \{v \in [L^2(\Omega_j)]^2 : \nabla\cdot v \in L^2(\Omega_j)\}$.

Let us denote by $(\cdot,\cdot)_j$ the usual complex inner product in $L^2(\Omega_j)$ and $\langle\cdot,\cdot\rangle_D$ the complex inner product in $L^2(D)$, being $D = \Gamma_j$ or $D = \Gamma_{jk}$.

Then, the equations (3.1) are multiplied by $v^s \in [H^1(\Omega_j)]^2$, $v^n \in H(div, \Omega_j)$ and $v^w \in H(div, \Omega_j)$, respectively, integrated over $\Omega_j$ and used integration by parts in the terms $(\nabla\cdot\tau(u_j), v^s)_j$, $(\nabla\mathcal{T}_n(u_j), v^n)_j$ and $(\nabla\mathcal{T}_w(u_j), v^w)_j$. After applying the boundary conditions (3.3) and (3.4), we obtain the domain decomposition iteration at the differential level: given $u_j^0 \in [H^1(\Omega_j)]^2 \times H(div, \Omega_j) \times H(div, \Omega_j)$ for all j, for $t = 1, 2, 3, \cdots$, find

$u_j^t \in [H^1(\Omega_j)]^2 \times H(div,\Omega_j) \times H(div,\Omega_j)$ such that

$$
\begin{aligned}
-\omega^2 \left(\rho\, u_j^{s,t} + \rho_n\, \bar{S}_n u_j^{n,t} + \rho_w\, \bar{S}_w\, u_j^{w,t},\ v^s\right)_j - \omega^2 \left(\rho_n\, \bar{S}_n\, u_j^{s,t} + g_n\, u_j^{n,t} + g_{nw}\, u_j^{w,t},\ v^n\right)_j \\
-\omega^2 \left(\rho_w\, \bar{S}_w\, u_j^{s,t} + g_{nw}\, u_j^{n,t} + g_w\, u_j^{w,t},\ v^w\right)_j + i\omega \left(d_n\, u_j^{n,t},\ v^n\right)_j \\
-i\omega \left(d_{nw}\, u_j^{w,t},\ v^n\right)_j + i\omega \left(d_w\, u_j^{w,t},\ v^w\right)_j - i\omega \left(d_{nw}\, u_j^{n,t},\ v^w\right)_j \\
+\sum_{pq} \left(\tau_{pq}(u_j^t),\ \varepsilon_{pq}(v^s)\right)_j - \left(\mathcal{T}_n(u_j^t),\ \nabla\cdot v^n\right)_j - \left(\mathcal{T}_w(u_j^t),\ \nabla\cdot v^w\right)_j \\
+\left\langle i\,\omega \mathcal{B}\big(u_j^{s,t}\cdot\nu_j, u_j^{s,t}\cdot\chi_j, u_j^{n,t}\cdot\nu_j, u_j^{w,t}\cdot\nu_j\big),\ \big(v^s\cdot\nu_j, v^s\cdot\chi_j, v^n\cdot\nu_j, v^w\cdot\nu_j\big)\right\rangle_{\Gamma_j} \\
+\sum_k \left\langle i\,\omega\beta_{jk}\big(u_j^{s,t}\cdot\nu_{jk}, u_j^{s,t}\cdot\chi_{jk}, u_j^{n,t}\cdot\nu_{jk}, u_j^{w,t}\cdot\nu_{jk}\big),\ \big(v^s\cdot\nu_{jk}, v^s\cdot\chi_{jk}, v^n\cdot\nu_{jk}, v^w\cdot\nu_{jk}\big)\right\rangle_{\Gamma_{jk}} \\
= (f^s,\ v^s)_j + (f^n,\ v^n)_j + (f^w,\ v^w)_j \\
-\sum_k \left\langle i\,\omega\beta_{jk}\left(u_k^{s,t-1}\cdot\nu_{kj}, u_k^{s,t-1}\cdot\chi_{kj}, u_k^{n,t-1}\cdot\nu_{kj}, u_k^{w,t-1}\cdot\nu_{kj}\right),\right. \\
\left.\big(v^s\cdot\nu_{jk}, v^s\cdot\chi_{jk}, v^n\cdot\nu_{jk}, v^w\cdot\nu_{jk}\big)\right\rangle_{\Gamma_{jk}} \\
-\sum_k \left\langle \left(-\tau_{pq}(u_k^{t-1})\nu_{kj}\cdot\nu_{kj},\ -\tau_{pq}(u_k^{t-1})\nu_{kj}\cdot\chi_{kj},\ \mathcal{T}_n(u_k^{t-1}),\ \mathcal{T}_w(u_k^{t-1})\right),\right. \\
\left.\big(v^s\cdot\nu_{jk}, v^s\cdot\chi_{jk}, v^n\cdot\nu_{jk}, v^w\cdot\nu_{jk}\big)\right\rangle_{\Gamma_{jk}}, \quad (v^s, v^n, v^w) \in [H^1(\Omega_j)]^2 \times H(div,\Omega_j) \times H(div,\Omega_j).
\end{aligned}
\tag{8}
$$

### 3.3 Iterative domain decomposition at the finite element level

Let $\mathcal{P}^h$ be a finite element partition of $\Omega$ into rectangles $\Omega_j$ of diameter bounded by $h$ that coincides with the domain decomposition partition $\Omega_j$.

The nonconforming finite element space used to obtain approximations to each component of the solid displacement vector $u_j^s$ in $\Omega_j$ is constructed using the following reference rectangular element

$$
\begin{aligned}
\widehat{R} = [-1,1]^2 \qquad V(\widehat{R}) = \text{Span}\Big\{ & \frac{1}{4} \pm \frac{1}{2}x - \frac{3}{8}\left((x^2 - \frac{5}{3}x^4) - (y^2 - \frac{5}{3}y^4)\right), \\
& \frac{1}{4} \pm \frac{1}{2}y + \frac{3}{8}\left((x^2 - \frac{5}{3}x^4) - (y^2 - \frac{5}{3}y^4)\right)\Big\},
\end{aligned}
$$

with the four degrees of freedom located at the mid points of the faces of $\widehat{R}$, i.e., the values at the nodal points $\xi^L = (-1,0), \xi^B = (0,-1), \xi^R = (1,0)$ and $\xi^T = (0,1)$. For

example the basis function $\varphi^L(x,z) = \frac{1}{4} - \frac{1}{2}x - \frac{3}{8}\left((x^2 - \frac{5}{3}x^4) - (z^2 - \frac{5}{3}z^4)\right)$ is such that $\varphi^L(\xi^L) = 1$ and $\varphi^L(\xi^l) = 0, l = B, R, T$. Similarly we construct the other three basis elements $\varphi^l, l = B, R, T$

To approximate the fluid displacement vectors $u_j^n$ and $u_j^w$ we choose the vector part of the Raviart-Thomas-Nedelec space of index 0 defined on $\widehat{R}$ as follows:

$$W(\widehat{R}) = \mathrm{Span}\{1, x\} \times \mathrm{Span}\{1, z\}.$$

The four degrees of freedom associated with each fluid displacement vector are the values of their horizontal components at $\xi^L, \xi^R$ and of their vertical components at $\xi^B, \xi^T$, or equivalently, the values of their normal components at the mid points of the faces of $\widehat{R}$.

The local basis are defined by

$$\psi^L(x) = -1 + x, \quad \psi^R(x) = x, \quad \psi^B(z) = -1 + z, \quad \psi^T(z) = z,$$

Next we can construct the subspaces $V_j^h = V(\Omega_j)$ and $W_j^h = W(\Omega_j)$ used to represent the approximating functions for the solid and fluid displacement vectors on each element $\Omega_j$.

In this stage we propose the so called hybrid formulation and introduce Lagrange multipliers, $\eta_{jk} = (\eta_{jk}^{s,\nu}, \eta_{jk}^{s,\chi}, \eta_{jk}^n, \eta_{jk}^w)$ for each subdomain associated with the values of the generalized forces at the mid points $\xi_{jk}$ of $\Gamma_{jk}$ that are used to "glue" the values in the interfaces:

$$\begin{gathered} \eta_{jk}^{s,\nu} \sim (\tau(u_j)\nu_{jk} \cdot \nu_{jk})(\xi_{jk}), \quad \eta_{jk}^{s,\chi} \sim \tau(u_j)\nu_{jk} \cdot \chi_{jk}(\xi_{jk}), \\ \eta_{jk}^n \sim \mathcal{T}_n(u_j)(\xi_{jk}), \quad \eta_{jk}^w \sim \mathcal{T}_w(u_j)(\xi_{jk}) \end{gathered} \tag{9}$$

This new set of Lagrange multipliers is:

$$\Lambda^h = \left\{ \eta \colon \eta|_{\Gamma_{jk}} = \eta_{jk} \in [P_0(\Gamma_{jk})]^4 = \Lambda_{jk}^h, \, \forall\{j,k\} \right\},$$

where $P_0(\Gamma_{jk})$ denotes the constant functions on $\Gamma_{jk}$.

The boundary integrals will be computed approximately using the mid–point quadrature: for $D = \Gamma_j$ and $D = \Gamma_{jk}$ we approximate $\langle u, v \rangle_D$ by

$$\langle\langle u, v \rangle\rangle_{\Gamma_{jk}} = (u\overline{v})(\xi_{jk})|\Gamma_{jk}|$$

where $|\Gamma_{jk}|$ is the measure of $\Gamma_{jk}$.

If, for $t = 0, 1, 2, \cdots$ we represent the finite element approximations of the displacement $U_j^{s,t}, U_j^{n,t}, U_j^{w,t}$ to $u_j^{s,t}, u_j^{n,t}, u_j^{w,t}$ and the Lagrange multipliers, $\eta_{jk}^t$, at the $t-$iteration level, we can finally define the three steps of our algorithm using (3.6), (3.4) and (3.7):
(1) Choose an initial guess $(U_j^0, \eta_{jk}^0) \in [V_j^h]^2 \times W_j^h \times W_j^h \times \Lambda_{jk}^h$

(2) For all $j$, compute $(U_j^t, \eta_{jk}^t) \in [V_j^h]^2 \times W_j^h \times \Lambda_{jk}^h$ as the solution of the equation

$$
\begin{aligned}
&-\omega^2 \left(\rho\, U_j^{s,t} + \rho_n\, \bar{S}_n U_j^{n,t} + \rho_w\, \bar{S}_w\, U_j^{w,t},\, v^s\right)_j - \omega^2 \left(\rho_n\, \bar{S}_n\, U_j^{s,t} + g_n\, U_j^{n,t} + g_{nw}\, U_j^{w,t},\, v^n\right)_j \\
&-\omega^2 \left(\rho_w\, \bar{S}_w\, U_j^{s,t} + g_{nw}\, U_j^{n,t} + g_w\, U_j^{w,t},\, v^w\right)_j + i\omega \left(d_n\, U_j^{n,t},\, v^n\right)_j \\
&-i\omega \left(d_{nw}\, U_j^{w,t},\, v^n\right)_j + i\omega \left(d_w\, U_j^{w,t},\, v^w\right)_j - i\omega \left(d_{nw}\, U_j^{n,t},\, v^w\right)_j \\
&+\sum_{pq} \left(\tau_{pq}(U_j^t),\, \varepsilon_{pq}(v^s)\right)_j - \left(\mathcal{T}_n(U_j^t),\, \nabla \cdot v^n\right)_j - \left(\mathcal{T}_w(U_j^t),\, \nabla \cdot v^w\right)_j \\
&+\left\langle\left\langle i\,\omega \mathcal{B}\big(U_j^{s,t}\cdot\nu_j, U_j^{s,t}\cdot\chi_j, U_j^{n,t}\cdot\nu_j, U_j^{w,t}\cdot\nu_j\big),\, \big(v^s\cdot\nu_j, v^s\cdot\chi_j, v^n\cdot\nu_j, v^w\cdot\nu_j\big)\right\rangle\right\rangle_{\Gamma_j} \\
&+\sum_k \left\langle\left\langle i\,\omega\beta_{jk}\big(U_j^{s,t}\cdot\nu_{jk}, U_j^{s,t}\cdot\chi_{jk}, U_j^{n,t}\cdot\nu_{jk}, U_j^{w,t}\cdot\nu_{jk}\big),\, \big(v^s\cdot\nu_{jk}, v^s\cdot\chi_{jk}, v^n\cdot\nu_{jk}, v^w\cdot\nu_{jk}\big)\right\rangle\right\rangle_{\Gamma_{jk}} \\
&= \left(f^s,\, v^s\right)_j + \left(f^n,\, v^n\right)_j + \left(f^w,\, v^w\right)_j \\
&-\sum_k \left\langle\left\langle i\,\omega\beta_{jk}\big(U_k^{s,t-1}\cdot\nu_{kj}, U_k^{s,t-1}\cdot\chi_{kj}, U_k^{n,t-1}\cdot\nu_{kj}, U_k^{w,t-1}\cdot\nu_{kj}\big),\right.\right. \\
&\qquad\left.\left.\big(v^s\cdot\nu_{jk}, v^s\cdot\chi_{jk}, v^n\cdot\nu_{jk}, v^w\cdot\nu_{jk}\big)\right\rangle\right\rangle_{\Gamma_{jk}}, \\
&-\sum_k \left\langle\left\langle\big(-\eta_{kj}^{s,\nu,t-1}, -\eta_{kj}^{s,\chi,t-1}, \eta_{kj}^{n,t-1}, \eta_{kj}^{w,t-1}\big), \big(v^s\cdot\nu_{jk}, v^s\cdot\chi_{jk}, v^n\cdot\nu_{jk}, v^w\cdot\nu_{jk}\big)\right\rangle\right\rangle_{\Gamma_{jk}}, \\
&(v^s, v^n, v^w) \in [V_j^h]^2 \times W_j^h \times W_j^h \times \Lambda_{jk}^h.
\end{aligned}
\tag{10}
$$

(3) Update the Lagrange multipliers $\eta_{jk}^t$.

$$
\begin{aligned}
\big(\eta_{jk}^{s,\nu,t}, \eta_{jk}^{s,\chi,t}, -\eta_{jk}^{n,t}, -\eta_{jk}^{w,t}\big) &= \big(\eta_{kj}^{s,\nu,t-1}, \eta_{kj}^{s,\chi,t-1}, -\eta_{kj}^{n,t-1}, -\eta_{kj}^{w,t-1}\big) \\
&- i\omega\beta_{jk}\Big(u_j^{s,t}\cdot\nu_{jk} + u_k^{s,t-1}\cdot\nu_{kj}, u_j^{s,t}\cdot\chi_{jk} + u_k^{s,t-1}\cdot\chi_{kj}, \\
&\qquad u_j^{n,t}\cdot\nu_{jk} + u_k^{n,t-1}\cdot\nu_{kj}, u_j^{w,t}\cdot\nu_{jk} + u_k^{w,t-1}\cdot\nu_{kj}\Big)(\xi_{jk})
\end{aligned}
\tag{11}
$$

The convergence for this iterative procedure is a consequence of the arguments given in.[35,36]

## 4 NUMERICAL RESULTS

Numerical results were obtained with a basic bidimensional model, a square of side length 6 cm, with 640 subdomains in both directions.

To simulate an experiment of ultrasonic wave transmission in a porous saturated rocks, we consider the following point source located at the center of the domain:

$$
\begin{aligned}
f^s(x,z,\omega) &= f^{s,P}(x,z,\omega) + f^{s,S}(x,z,\omega) \\
&= \Big(\frac{\partial \delta_{x-x_s,z-z_s}}{\partial x}, \frac{\partial \delta_{x-x_s,z-z_s}}{\partial z}\Big)\ g(\omega) + \Big(\frac{\partial \delta_{x-x_s,z-z_s}}{\partial z}, \frac{\partial \delta_{x-x_s,z-z_s}}{\partial x}\Big)\ g(\omega) \\
f^n(x,z,\omega) &= f^w(x,z,\omega) = \Big(\frac{\partial \delta_{x-x_s,z-z_s}}{\partial x}, \frac{\partial \delta_{x-x_s,z-z_s}}{\partial z}\Big)\ g(\omega),
\end{aligned}
$$

where $f^{s,P}(x,z,\omega)$ and $f^{s,S}(x,z,\omega)$ represent the compressional and shear parts applied to the solid matrix and $f_0$ denotes the principal frequency of the external source chosen to be 500 KHz. Here $g(\omega)$ is the Fourier transform of

$$
g(t) = -2\xi(t-t_0)e^{-\xi(t-t_0)^2},
$$

with $\xi = 8\ f_0^2$ and $t_0 = 1.25/f_0$.

The displacements $u^s(x,z,t)$, $u^n(x,z,t)$ and $u^w(x,z,t)$ were calculated using the iterative method (3.8)–(3.9) for 100 frequencies in the interval (0, 1000) KHz. The solution in the space–time domain was obtained through the discrete inverse Fourier transform and the error of this approximation is proportional to $(h + (\Delta\omega)^2)$.[18]

We consider propagation of waves in a sample of Nivelsteiner sandstone whose material properties are given in Table 1,,[12] the viscoelastic parameters that describe the dissipative behaviour and the physical properties of the saturant fluids are also indicated. The reference fluid pressure is 30 MPa, corresponding to the normal hydrostatic pressure at a burial depth of about 3 km.

The capillary pressure function and the permeability functions are taken from the article by Douglas et al.[37] who correlated experimental data for a variety of porous rocks.

The phase velocities and attenuation coefficients at the principal frequency $f_0$ are given in Table 2, where we compare the values corresponding to the poroelastic and poroviscoelastic formulations. Here, the pore space is assumed to be filled by 90% water (as the wetting phase) and 10 % of hydrocarbon gas.

A snapshot of the vertical component of the particle velocity ($V(x,z,t) = \frac{\partial U(x,z,t)}{\partial t}$) at a propagating time of 0.018 msec for the solid matrix is shown in Figure 1. The wavefronts related to the three compressional modes (labeled P1, P2 and P3) and the shear mode (labeled S) can be observed. This figure also illustrates the effectiveness of the absorbing boundary conditions since the Type I-wave front is passing through the domain without artificial reflections.

In addition, the analysis of different snapshots showed that the amplitudes of the two slow modes (Type II and Type III) are much stronger in the fluid media and the amplitude of Type III waves decrease notably with respect to the amplitude of Type II waves while time pass.

Table 1: Material properties for Nivelsteiner sandstone

| | | |
|---|---|---|
| *Grain* | density, $\rho_s$ | 2.65 gr/cm$^3$ |
| | bulk modulus | 36 GPa |
| *Matrix* | porosity, $\phi$ | 33 % |
| | bulk modulus | 6.21 GPa |
| | absolute permeability | 5000 mDarcy |
| | shear modulus, $N$ | 4.55 GPa |
| | bulk loss, $Q_p$ | 30 |
| | shear loss, $Q_s$ | 20 |
| *Gas* | density, $\rho_n$ | 0.1 gr/cm$^3$ |
| | viscosity | 0.00015 Poise |
| | bulk modulus | 0.022 GPa |
| *Water* | density, $\rho_w$ | 1 gr/cm$^3$ |
| | viscosity | 0.01 Poise |
| | bulk modulus | 2.223 GPa |

Table 2: Phase velocities and attenuation coefficients at 500 KHz and gas saturation 10 %

| *Wave* | *Poro-elastic phase velocity, [km/sec]* | *Poro-elastic attenuation factor, [DB]* |
|---|---|---|
| *P1* | 2.5454028 | 0.10571459 |
| *P2* | 0.27500635 | 1.3678229 |
| *P3* | 0.41792553 | 2.4865442 |
| *S* | 1.5323432 | 0.12485457 |
| *Wave* | *Poro-viscoelastic phase velocity, [km/sec]* | *Poro-viscoelastic attenuation factor, [DB]* |
| *P1* | 2.5299388 | 1.2232244 |
| *P2* | 0.27498727 | 1.3839098 |
| *P3* | 0.41790992 | 2.4968665 |
| *S* | 1.5212897 | 1.4605364 |

In the next figure, we plot traces of the vertical component of the total particle velocity $V_z^T = V_z^s + S_n V^n + S_w V^w$ at a receiver located at $x = 4$ cm, $z = 3.5$ cm with normalized amplitude. Our aim is to analyze the influence of the porosity on the amplitudes of the different waves. From the figures 2 a) and b) we observe that an increment in porosity from 0.33 to 0.55 produces greater amplitudes in the slow modes. The differences in the arrival times due to the changes of phase velocities can also be noted.

In the figures 3 and 4 we show traces of the divergence of the particle velocities of the solid, nonwetting and wetting fluid phases for two different saturations. We restrict our attention to the slow waves for analyzing the relative motion between the different phases. Figure 3 a) and b) illustrates the normalized traces of the solid vs. the nonwetting fractions (first normalized to the maximum value of the fluid phase, and then, the solid-phase trace is scaled by factors of 282 for $S_n = 0.1$ and 4240 for $S_n = 0.4$), where in both we can see the motion in opposite phase for the Type II and III waves.

Finally, in figure 4 a) and b) we plot the normalized traces of the wetting vs. the nonwetting fluids (first normalized to the maximum value of the non-wetting phase, and then, the wetting-phase trace is scaled by a factor of 3.5 for $S_n = 0.1$ and 5.5 for $S_n = 0.4$)). It must be remarked that for the slowest mode (Type II) both fluids move in phase and the contrary holds for the other mode. For this reason we conclude that this Type II wave corresponds to the classic slow Biot's wave. Moreover, the greater content of gas increases notably the amplitudes of the Type III wave in both fluids while the opposite effect can be observed in the other slow wave.

## 5 CONCLUSIONS

We have proposed an algorithm formulated in the space–frequency domain to simulate the propagation of waves in a bounded poroviscoelastic solid saturated by two immiscible fluids. The model is a generalization of the classical Biot's theory for single–phase fluids taking into account capillary forces and viscous and mass coupling interaction coefficients between the fluid phases under variable saturation and pore fluid pressure conditions with corrections for high frequencies.

In the space–frequency domain each temporal frequency could be solved independently of the other frequencies and the time–domain solution was obtained by an approximate inverse Fourier transform.

We implemented an iterative nonoverlapping domain decomposition method that employs an absorbing boundary condition in order to minimize spurious reflections from the artificial boundaries and that is specifically designed for parallel architectures.

The numerical simulation of waves in a real sandstone saturated by gas–water showed the existence of a second slow compressional wave (called Type III) at ultrasonic frequencies under normal hydrostatic fluid pressures. In these experiments we observed that the two slow compressional waves have phase velocities on the same order of magnitude. In addition, our results demonstrated the great influence of parameters such as porosity and saturation on the amplitudes and the arrival times of the different kind of waves.

It is remarked that this modelling method may be useful for developing suitable laboratory experiments and so the second slow wave should be observed.

## REFERENCES


[1] M. A. Biot. Theory of propagation of elastic waves in a fluid-saturated porous solid. 1. low frequency range. *J. Acoust. Soc. Am.*, **28**, 168–171 (1956).

[2] M. A. Biot. Theory of propagation of elastic waves in a fluid-saturated porous solid. 2. high frequency range. *J. Acoust. Soc. Am.*, **28**, 179–191 (1956).

[3] M. A. Biot. Mechanics of deformation and acoustic propagation in porous media. *J. Appl. Phys.*, **33**, 1482–1498 (1962).

[4] J. Berryman, L. Thigpen, and R. Chin. Bulk elastic wave propagation in partially saturated porous solids. *J. Acoust Soc. Am.*, **84**, 360–373 (1988).

[5] N. C. Dutta and H. Odé. Attenuation and dispersion of compressional waves in fluid-filled porous rocks with partial gas saturation (white model) – part i: Biot theory. *Geophysics*, **44**, 1777–1788 (1979).

[6] S. Mochizuki. Attenuation in partially saturated rocks. *J. of Geophys. Res.*, **87**, 8598–8604 (1982).

[7] M. N. Toksöz, C. H. Cheng, and A. Timur. Velocities of seismic waves in porous rocks. *Geophysics*, **41**, 621–645 (1976).

[8] M. A. Biot. Theory of deformation of a porous viscoelastic anisotropic solid. *J. Appl. Phys.*, **27**, 459–467 (1956).

[9] T. J. Plona. Observation of a second bulk compressional wave in a porous medium at ultrasonic frequencies. *Appl. Phys. Lett.*, **56**, 259–261 (1980).

[10] J. Douglas Jr., J. E. Santos, and J. L. Hensley. Simulation of biot waves in a cylindrically symmetric domain. *Proceedings of the Third International Conference on Hyperbolic Problems, (B. Engquist and B. Gustafson, eds.), Chartwell-Bratt*, **1**, 330–350 (1990).

[11] J. L. Hensley, J. Douglas Jr., and J. E. Santos. Dispersion of type ii biot waves in inhomogeneous media. *Proceedings of the 6th. International Conference on Mathematical Methods in Engineering, Czechoslovakia*, **1**, 67–83 (1991).

[12] B. Arntsen and J. M. Carcione. Numerical simulation of the biot slow wave in water-saturated nivelsteiner sandstone. *Geophysics*, **66**, 890–896 (2001).

[13] J. M. Carcione and G. Quiroga-Goode. Some aspects of the physics and numerical modeling of biot compressional waves. *J. Comput. Acous.*, **3**, 261–280 (1996).

[14] J. E. Santos, J. Douglas Jr., J. M. Corberó, and O. M. Lovera. A model for wave propagation in a porous medium saturated by a two–phase fluid. *J. Acoust. Soc. Amer.*, **87**, 1439 (1990).

[15] J. E. Santos, J. Douglas Jr., and J. Corberó. Static and dynamic behaviour of a porous solid saturated by a two-phase fluid. *J. Acoust. Soc. Am.*, **87**, 1428 (1990).

[16] J. E. Santos and C. L. Ravazzoli. Behavior of porous solid saturated by a two-phase fluid under variable pressure conditions. *submitted to J. Acoust. Soc. Am.*

[17] J. Douglas Jr., J. E. Santos, and D. Sheen. Approximation of scalar waves in the space-frequency domain. *Math. Models Methods App. Sci.*, **4**, 509–531 (1994).

[18] J. Douglas Jr., J. E. Santos, D. Sheen, and L. Bennethum. Frequency domain treatment of one–dimensional scalar waves. *Math. Models Methods App. Sci.*, **3**, 171–194 (1993).

[19] P. M. Gauzellino, J. E. Santos, and D. Sheen. Frequency domain wave propagation modelling in exploration seismology. *J. Comput. Acous.*, **9**, 941–955 (2001).

[20] P. L. Lions. On the schwarz alternating method, i. *Domain Decomposition Methods for Partial Differential Equations, R. Glowinski and G. Golub and G. Meurant and J. Périaux (eds.) (SIAM, Philadelphia)*, pages 1–42 (1988).

[21] P. L. Lions. On the schwarz alternating method, iii: a variant for nonoverlapping subdomains. *Proceedings of the Third International Symposium on Domain Decomposition Methods for Partial Differential Equations, T. F. Chan and R. Glowinski and J. Périaux and O. B. Widlund (eds.) (SIAM, Philadelphia*, pages 202–223 (1990).

[22] B. Després. Méthodes de décomposition de domaines pour les problèmes de propagation d'ondes en régime harmonique. *Thèse, Université Paris IX Dauphine, UER Mathématique de la Décision*, (1991).

[23] B. Després, P. Joly, and J. E. Roberts. A domain decomposition method for the harmonic maxwell equations. *Iterative Methods in Linear Algebra, R. Beauwens and P. de Groen, (eds.), Elsevier Science Publishers B. V. (North-Holland), Amsterdam*, pages 475–484 (1992).

[24] J. Douglas Jr, P. L. Paes Leme, J. E. Roberts, and J. Wang. A parallel iterative procedure applicable to the approximate solution of second order partial differential equations by mixed finite element methods. *Numer. Math.*, **65**, 95–108 (1993).

[25] J. Douglas Jr., F. Pereira, and J. E. Santos. A domain decomposition approach to the simulation of waves in dispersive media. *Proceedings of the Third International Conference on Wave Propagation Phenomena, G. Cohen, (ed.), SIAM, Philadelphia*, pages 673–682 (1995).

[26] J. Douglas Jr., J. E. Santos, D. Sheen, and X. Ye. Nonconforming galerkin methods based on quadrilateral elements for second order elliptic problems. *RAIRO Mathematical Modelling and Numerical Analysis (M2AN)*, **33**, 747–770 (1999).

[27] P. A. Raviart and J. M. Thomas. Mixed finite element method for 2-nd order elliptic problems. *Mathematical Aspects of the Finite Element Methods, Lecture Notes of Mathematics*, **606** (1975).

[28] J. C. Nedelec. Mixed finite elements in $r^3$. *Numer. Math.*, **35**, 315–341 (1980).

[29] J. E. Santos, C. L. Ravazzoli, P. M. Gauzellino, J. M. Carcione, and F. Cavallini. Simulation of waves in poro-viscoelastic rocks saturated by immiscible fluids. numerical evidence of a second slow wave. *submitted to J. Acoust. Soc. Am.*

[30] J. Bear. *Dynamics of fluids in porous media.* Dover Publications, New York, (1972).

[31] D. W. Peaceman. *Fundamentals of numerical reservoir simulation.* Elsevier, (1977).

[32] A. E. Scheidegger. *The physics of flow through porous media.* University of Toronto,

Toronto, (1974).

[33] H. P. Liu, D. L. Anderson, and H. Kanamori. Velocity dispersion due to anelasticity; implications for seismology and mantle composition. *Geophys. J. R. Astr. Soc.*, **147**, 41–58 (1976).

[34] D. Sheen. Finite element methods for an acoustic well-logging problem associated with a porous medium saturated by a two–phase immiscible fluid. *Numerical Methods for Partial Differential Equations*, **9**, 155–174 (1993).

[35] J. Douglas Jr., J. E. Santos, and D. Sheen. Nonconforming galerkin methods for the helmholtz equation. *Numerical Methods for Partial Differential Equations*, **17**, 475–494 (2001).

[36] T. Ha, J. E. Santos, and D. Sheen. Nonconforming finite element methods for the simulation of waves in viscoelastic solids. *to appear in Computer Methods in Applied Mechanics and Engineering.*

[37] J. Douglas Jr, J. L. Hensley, and P. J. Paes Leme. A study of the effect of inhomogeneities on immiscible flow in naturally fractured reservoirs. *International Series of Numerical Mathematics (Birkhauser Verlag Basel)*, **114**, 59–74 (1993).

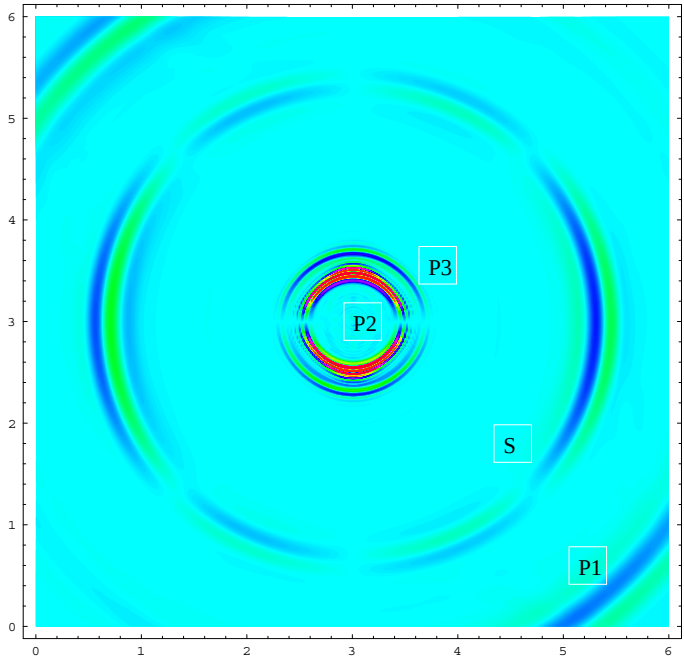


Figure 1: Snapshot of the vertical component of the particle velocity of the solid part at time $t = 0.018$ msec

a) Porosity=0.33

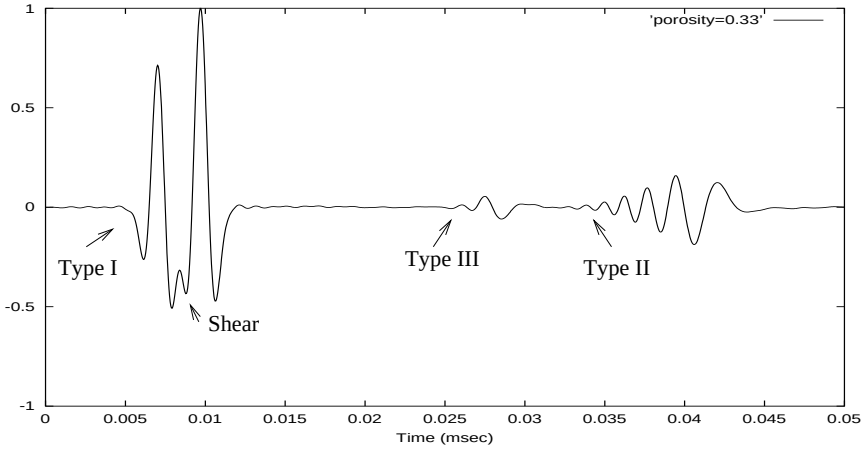


b) Porosity=0.55

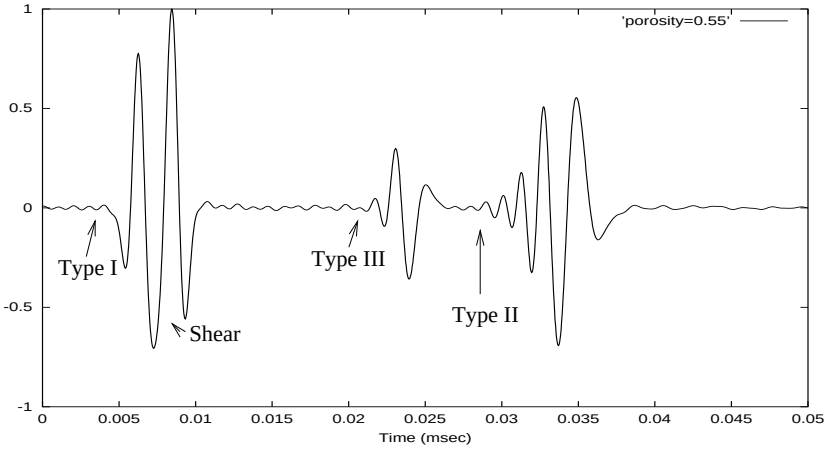


Figure 2: Normalized traces of vertical component of the total particle velocity at a receiver located at $x = 4$ cm, $z = 3.5$ cm

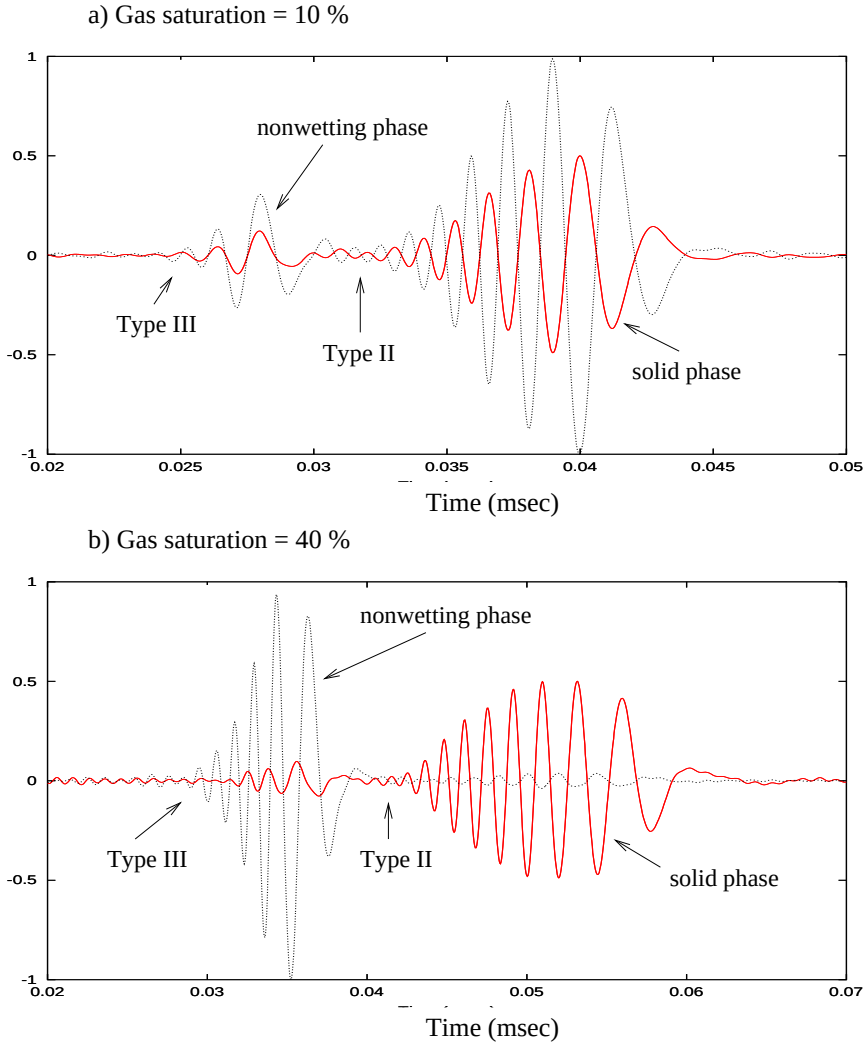


Figure 3: Traces of divergence of the particle velocity of the solid and nonwetting fluid phases at a receiver located at $x = 4$ cm, $z = 3.5$ cm

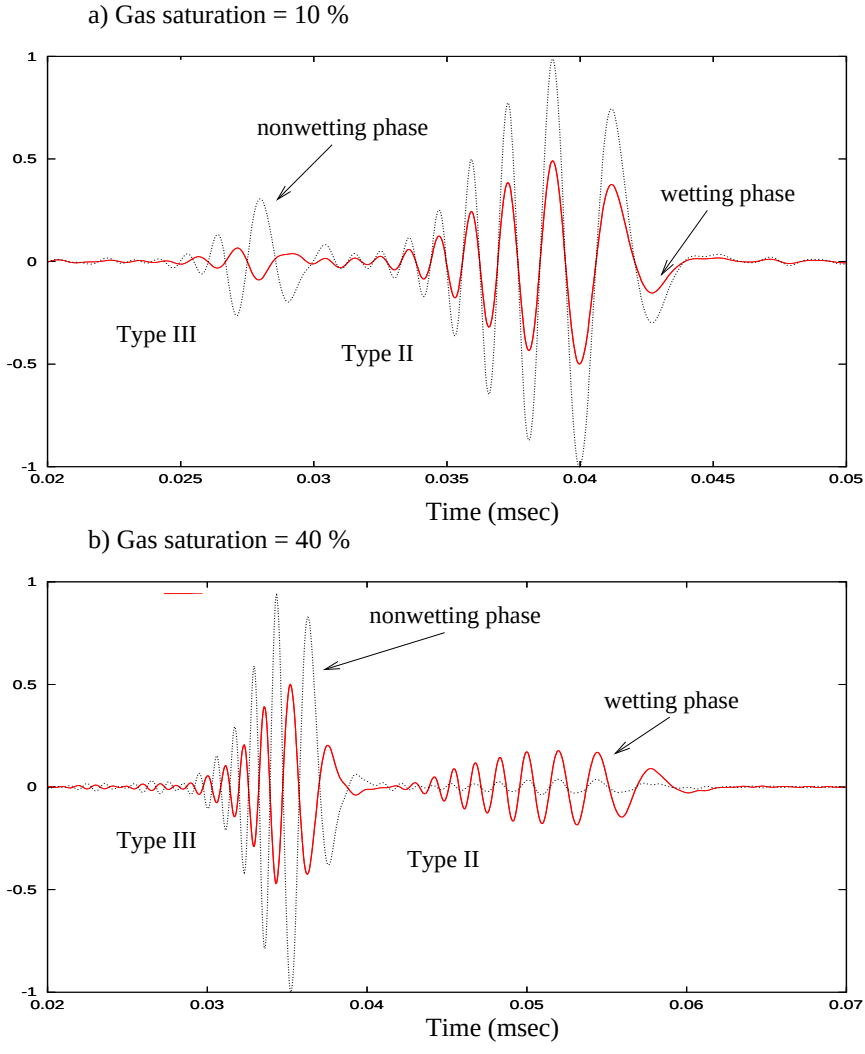


Figure 4: Traces of divergence of the particle velocity of the wetting and nonwetting fluid phases at a receiver located at $x = 4$ cm, $z = 3.5$ cm